# Oxygen Storage in Stacked Phospholipid Membranes Under an Oxygen Gradient as a Model for Myelin Sheaths

Wouter Vervust and An Ghysels

## Abstract

Axons in the brain and peripheral nervous system are enveloped by myelin sheaths, which are composed of stacked membrane bilayers containing large fractions of cholesterol, phospholipids, and glycolipids. The oxygen availability to the nearby oxygen consuming cytochrome $c$ oxidase in the mitochondria is essential for the well-functioning of a cell. By constructing a rate network model based on molecular dynamics simulations, and solving it for steady-state conditions, this work calculates the oxygen storage in stacked membranes under an oxygen gradient. It is found that stacking membranes increases the oxygen storage capacity, indicating that myelin can function as an oxygen reservoir. However, it is found that the storage enhancement levels out for stacks with a large number of bilayers, suggesting why myelin sheaths consist of only 10–300 membranes rather than thousands. The presence of additional water between the stacked bilayers, as seen in cancer cells, is shown to diminish myelin oxygen storage enhancement.

## 1 Introduction

The transport of molecular oxygen throughout the body is primarily realised by blood cells in the cardiovascular system [1]. The final destination of oxygen is the cytochrome $c$ oxidase (COX), a protein embedded in the inner mitochondrial membrane, where oxygen is consumed in the energy conversion cycle. The binding site for oxygen is located at the center of the inner mitochondrial membrane [2]. Passive diffusive transport through several membranes, including the plasma membrane, is responsible for the last steps of oxygen from blood cells to the COX binding site. Cancer cells are known to show hypoxia which can fluctuate across the tumour cell, and tumour oxygenation can enhance radiation therapy of cancer cells [3]. Interestingly, nerve cell axons are surrounded by myelin, which is composed of stacked membrane bilayers containing large fractions of cholesterol, phospholipids, and glycolipids [4, 5]. Understanding the mechanisms of oxygen pathways from capillaries to tissue mitochondria is thus important for completely unraveling the physiological role of oxygen [6].

W. Vervust · A. Ghysels (✉)
IBiTech – Biommeda research group, Ghent University, Ghent, Belgium
e-mail: an.ghysels@ugent.be

In this paper, a bottom-up approach will be used to study the role of membranes starting from the molecular scale. Phospholipid membranes form a barrier for oxygen, but the oxygen solubility in the phospholipid tail region is higher than in water, such that a high concentration of oxygen is found in the hydrophobic matrix [7, 8]. This high partitioning toward the membrane suggests that the omnipresence of phospholipid membranes provides the cell with an oxygen reservoir. Therefore, this paper wants to establish the view that a phospholipid membrane has a dual function: slowing oxygen transport, while also storing oxygen. Moreover, the inhomogeneity and anisotropy of the membrane facilitate oxygen transport in the interleaflet region of a lipid bilayer, compared to the transport orthogonal to the membrane surface [9]. The interleaflet space of bilayers can thus form a connected network of efficient diffusive pathways throughout the cell. The timely delivery of oxygen is especially important in the brain and the peripheral nervous system. This paper will in addition investigate how stacked membranes can serve as an oxygen reservoir in the nervous system, given a certain partial oxygen pressure.

In the methods section, kinetic modelling based on the Smoluchowski equation is introduced. It is explained how kinetic parameters were extracted from previous molecular dynamics (MD) simulations. The kinetic parameters will be used to predict the steady-state oxygen distribution given an oxygen gradient. In the results and discussion section, the enhancement in oxygen storage due to the stacking will be computed, where the number of stacked bilayers is varied. The conclusion section summarises our findings.

## 2    Methodology

**Smoluchowski Equation for Transport**  Due to the membrane's inhomogeneity along the membrane's normal (z-coordinate, Fig. 1), the oxygen concentration $c$ is $z$-dependent. It relates to the free energy profile $F(z) = -k_BT\ln c(z)$, with $k_B$ the Boltzmann constant and $T$ the temperature.

Diffusive transport through an inhomogeneous medium is governed by the Smoluchowski equation, which is determined by the free energy $F(z)$ and diffusion $D(z)$ profiles [10]. Discretisation in $N$ bins along $z$ transforms the Smoluchowski equation into a set of linearly coupled equations, which can be summarised by a rate model with rate matrix $R$

$$\frac{\partial c_i(t)}{\partial t} = \sum_{N}^{j=1} R_{ij} c_j(t),$$
(1)

where $c_i(t)$ is the concentration in bin $i$ at time $t$, and where the kinetic parameters in the rate matrix $R$ are uniquely determined by the $F(z)$ and $D(z)$ profiles [10]. In this work, we will solve the rate equations with different profiles, representing different stacked bilayers.

**Construction of the Rate Model from Molecular Simulations**  Bayesian analysis (BA) of MD trajectories at the atomic scale can be used to obtain the $F$ and $D$ profiles – and thus the rate matrix $R$ – of a membrane [9–11]. In practice, the transitions observed in conventional MD trajectories are compared to the transitions expected by the rate model with a proposed rate matrix $R$. A Monte Carlo procedure is then used to extract the rate matrix with the highest likelihood of producing the observed MD trajectories.

Previously published MD simulations and their $F$ and $D$ profiles are used in this work to investigate the storage capacity of stacked bilayers. The considered membranes are a homogeneous 1-palmitoyl-2-oleoyl-sn-glycero-3-phosphocholine (POPC) bilayer (see Fig. 1) and a model system for inner mitochondrial membrane (labeled MITO) from Ref. [9]. MD simulations were run with the CHARMM36 force field at 310 K with a simulation box containing 72 lipid molecules, as depicted in Fig. 1a [12, 13]. The $z$-axis was discretised into 100 bins ($z \oplus 0.68^-$), and BA was performed on the oxygen trajectories, resulting in the $F$ and $D$ profiles shown in Fig. 1b, c.

In a next step, the single-membrane profiles are extended to artificially construct the $F$ and $D$ profiles of $n$ stacked membranes by concatenat-
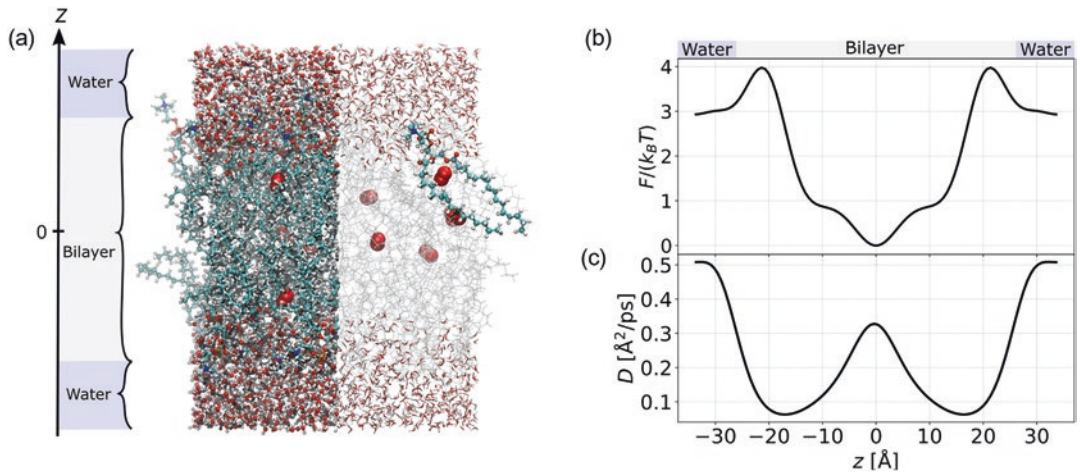
**Fig. 1** MD simulations of the (POPC) membrane. (**a**) Simulation box with indication of the $z$-axis. For clarity, water and phospholipid molecules are shaded in the right part of the box with one high-lighted POPC molecule (ball-and-stick) and red oxygen molecules (van der Waals spheres). (**b**) Free energy $F(z)$ in units $k_B T$. (**c**) Diffusivity $D(z)$. $F(z)$ and $D(z)$ were obtained from Bayesian analysis of the MD trajectories

ing the membrane part of the profiles $n$ times, to imitate myelin sheaths (Fig. 2a). The following three configurations are compared (Fig. 2b):

1. A water layer without any membrane (Fig. 2b top), representing oxygen diffusion to the mitochondria without shielding of membranes.
2. A single bilayer and water (Fig. 2b centre).
3. A series of $n$ stacked bilayers (Fig. 2b bottom), representing myelin sheaths.

The oxygen storage $S$ is measured under an oxygen gradient (see below), which gives $S(0)$, $S(1)$ and $S(n)$ for the setups with zero, one, and $n$ bilayers, respectively. The amount of water is varied in setup 1 and setup 2 to match the size of setup 3, as is depicted in Figs. 2b. This allows for comparison between equally sized configurations in the results and discussion section. The stacking periodicity $d$ can be increased to simulate a more disorganised structure with a larger aqueous phase between the membrane layers.

**Steady-State Solution Under Oxygen Gradient** The oxygen storage $S$ in the membranes is measured under an oxygen gradient, where one side (to the left in Fig. 2) has a partial

oxygen pressure and the other side (to the right of Fig. 2) has zero partial oxygen pressure, referring to full depletion of oxygen by COX. The concentration profile is assumed to have reached the steady-state regime, where the concentration no longer changes over time, but a net oxygen flux might still occur.

We solve the rate model (Eq. 1) for the steady-state solution, i.e., the right hand side of Eq. 1 vanishes, with bin 1 (to the left) at fixed concentration $c_1 = c^*$ and bin $N$ (to the right) at fixed concentration $c_N = 0$, for all times $t$. This is done by constructing the vector $v$ of length $N - 2$, which has all elements equal to zero except for its first element $v_1 = -R_{2,1}$. The rate matrix is stripped of its first and $N^{th}$ rows and columns, to form the cropped rate matrix $R'$ [14]. The steady-state concentration $c_i^{ss}$ in each bin $i$ is then obtained by matrix multiplication of $R'$ and the vector $v$, and scaling with the concentration $c^*$,

$$c_i^{ss} = \begin{cases} c^*, & i = 1 \\ c^* \sum_{j=2}^{N-1} \left[ R'^{-1} \right]_{i-1, j-1} v_j, & i = 2, \ldots, N-1 \\ 0, & i = N \end{cases} \quad (2)$$

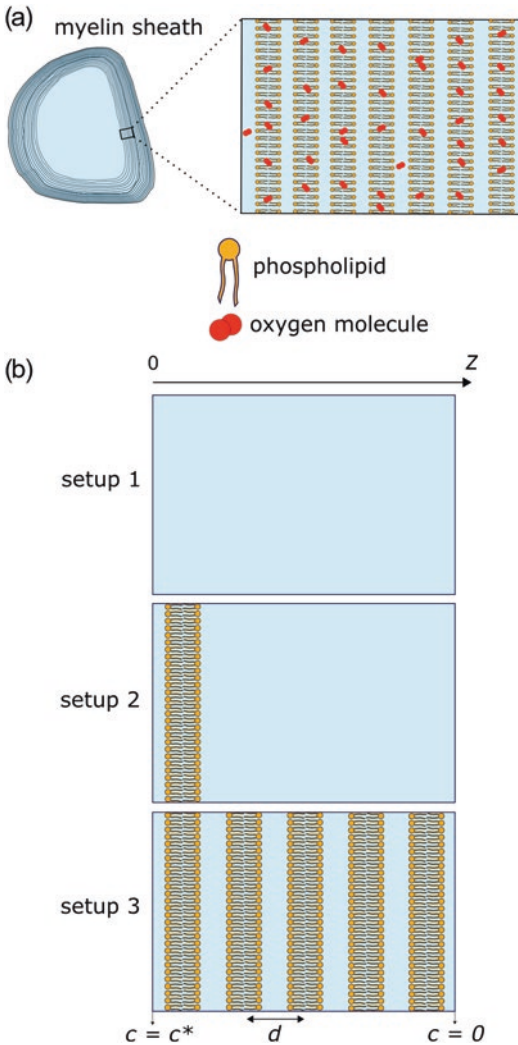**Fig. 2** (**a**) Myelin sheaths wrapped around a neural cell consist of stacked membranes [5]. (**b**) Considered configurations with steady-state boundary conditions: $c = c^*$ to the left and $c = 0$ to the right. Setup 1 is pure water, setup 2 has one bilayer, setup 3 has $n$ bilayers (depicted is $n = 5$). Stacking periodicity $d$ is indicated with arrow

where $R'^{-1}$ is the matrix inverse of $R'$. Finally, the storage capacity $S$ corresponding to a concentration profile $c(z)$ is computed by integrating over the concentration profile and multiplying with the membrane surface area $A$,

$$S = A \int c(z) dz \approx A \sum_i c_i \; z \qquad (3)$$

where in the second equation, the integral was approximated by the discretisation with bin width $\Delta z$.

# 3    Results and Discussion

First, we calculated the concentration profile under an oxygen gradient (Eq. 2) in the setups without bilayer, with one bilayer, and with $n$ stacked bilayers. The steady-state profiles for the POPC membrane are shown for $n = 5$ in Fig. 3a. The setup of pure water gives a simple linear slope (black line), while the presence of a membrane clearly introduces a high peak in oxygen concentration (blue dashed line). Increasing the number of stacked membranes creates additional peaks (green line), whose height drops linearly with each additional peak.

The stacking enhancement of adding bilayers is quantified by $E(n) = S(n)/S(1)$, which is the ratio between storage in $n$ stacked bilayers versus storage in 1 bilayer (setup 2 and setup 3 in Fig. 2). The membrane area $A$ (Eq. 3) drops out of this ratio, and $E(n)$ has no unit. Fig. 3b depicts the stacking enhancement $E(n)$ for the POPC and MITO membranes, which shows that the stacking enhancement increases with the number $n$ of stacked membranes. This indeed suggests that myelin sheaths may function as a reservoir for oxygen storage in the nervous system, making oxygen readily available to COX in the nearby mitochondria.

Interestingly, stacked bilayers not only have more peaks in Fig. 3a, but the first peak of the stacked bilayers (green) is also higher compared to the case of a single bilayer (blue dashed). This again favours the enhancement in stacked membranes compared to a single bilayer. The higher peak is explained by the fact that the nearby second peak also provides a source of oxygen.

Moreover, the slope of the curve in Fig. 3b becomes less steep with increasing $n$, meaning that stacking an additional membrane onto a thick layer of stacked membranes has less impact. In other words, stacking a 51st membrane on top of 50 stacked membranes has less impact on the stacking enhancement than stacking an 11th membrane on top of 10 stacked membranes. Therefore, it seems plausible that, for a certain stacking number, a trade-off may be reached between stacking enhancement and the extent of the physical space occupied by the membranes. Indeed, in electron microscopy images, myelin
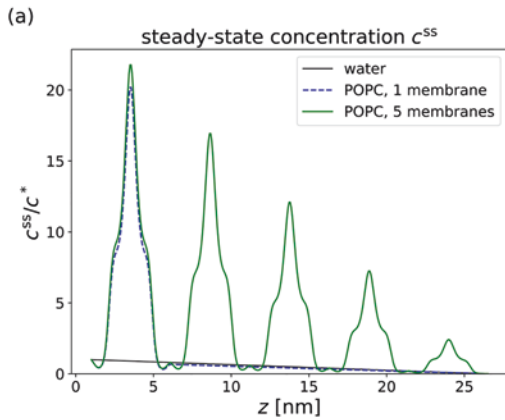
**Fig. 3** (a) Steady-state concentration profile under oxygen gradient (in units $c^*$) with $c = c^*$ to the left and $c = 0$ to the right, for $n = 5$. Setup 1 with only water (black), setup 2 with 1 POPC membrane (blue dashed) and setup 3 with $n = 5$ stacked POPC membranes (green), as shown in
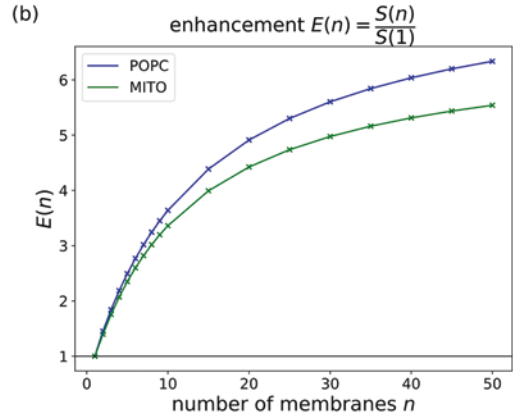
Fig. 2b. (b) Stacking enhancement $E(n) = S(n)/S(1)$ is the ratio of storage capacity between n stacked bilayers and one bilayer, under a steady-state oxygen gradient over the membrane(s). $S(1)$ and $S(n)$ correspond to setup 2 and setup 3 in Fig. 2, respectively

sheaths often consist of about 10–300 bilayers but not thousands [5].

The storage efficiency also depends on the intrinsic storage capacity of a single bilayer. The ratio $S(1)/S(0)$ is a measure for the content in a single bilayer compared to a slab of pure water with the same dimension. For POPC, this ratio amounts to $S(1)/S(0) \approx 8$ in the steady-state regime using a membrane thickness of approximately 5.2 nm. Because of the linearity of the rate model and the symmetry of the considered setups, we can conclude that the latter ratio is equivalent to the ratio of storage in a membrane versus storage in the water phase in equilibrium. This is also known as the membrane partitioning constant $K_m$, of which the study was initiated over a century ago with Overton's rule. In short, $S(1)/S(0) = K_m = c_{mem}/c_{wat}$, with $c_{mem}$ and $c_{wat}$ the equilibrium oxygen concentration in the membrane and water phase, respectively.

Concretely, the POPC membrane stores about 8 times more oxygen molecules than can be stored in pure water. For example, let us assume a partial oxygen pressure of ~10 mmHg, which lies in the reported 10–34 mmHg range for brain tissue [15]. At atmospheric pressure and body temperature, the partial oxygen pressure is 159 mmHg, and the solubility of oxygen in water is approximately 7.187 mg/L [16]. Therefore, the

10 mmHg partial oxygen pressure corresponds to an oxygen concentration of $(10/159) \cdot 7.187$ mg/L = 0.45 mg/L. Next, the steady-state profile over 10 stacked POPC membranes under this oxygen gradient ($c^* = 0.45$ mg/L to the left of the stack, while $c = 0$ to the right of the stack) is computed with Eq. 2, and similarly for pure water. Finally, the storage per area ($S/A$) follows from Eq. 3, resulting in about 1791/µm$^2$ oxygen molecules available in the membrane stack, compared to 226/µm$^2$ oxygen molecules in a similarly sized slab of water.

Next, it is tested how the bilayer spacing influences the enhancement provided by the stacked membranes. The pathophysiology of cancer cells may show abnormal microvasculature and defective microcirculatory function, such as an increase in interstitial fluid [17, 18]. Moreover, abnormal myelination can also occur following trauma to a central nervous system tract, where myelin sheath swelling and decompaction have been observed, even in myelin that is spatially separated from the primary injury [19, 20]. Here, structural loss in the membrane stacking is modeled by increasing the thickness of the aqueous phase between the stacked bilayers. These additional water layers will decrease the total permeability [21], but they might also affect the storage capacity. Fig. 4 shows the

**Fig. 4** Enhancement $S(n)/S(0)$ in stacked membranes for $n = 10$, as a function of stacking periodicity $d$
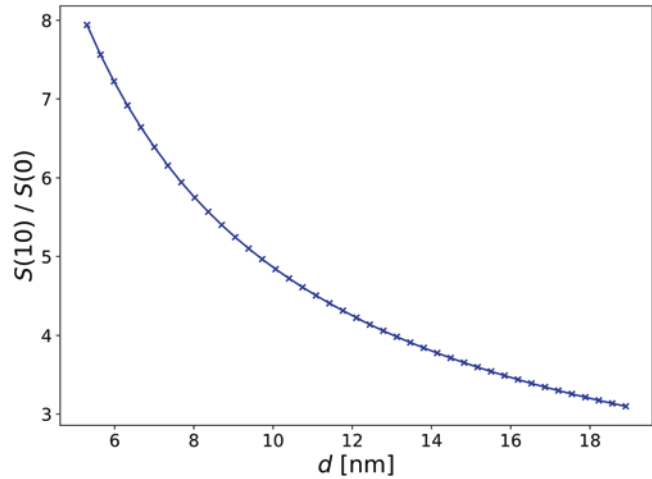


enhancement $S(n)/S(0)$ for $n = 10$ stacked bilayers, comparing the storage in 10 bilayers with the storage in pure water, while the stacking periodicity $d$ (indicated in Fig. 2b) is gradually increased. At the left of the figure, the periodicity $d = 5.2$ nm corresponds to 10 stacked POPC membranes without additional water, as was simulated in Fig. 3b. Figure 4 clearly shows that an increase in stacking periodicity $d$ can cause a strong decrease in the storage enhancement by the stacked bilayers, indicating that additional water between the myelin layers affects the storage efficiency in a negative way. This can be understood by comparing the contributions to the total storage by the membrane and by the interstitial water. The oxygen storage in water becomes larger for increasing $d$, simply because there is more interstitial water. In contrast, the oxygen storage in the membranes is fairly independent of $d$. Thus, for increasing periodicity $d$, the relative contribution of the bilayers to the total oxygen storage becomes smaller, and consequently a highly distorted membrane stack will gradually lose its function as a compact oxygen reservoir.

## 4    Conclusion

A phospholipid membrane has a higher solubility for molecular oxygen compared to pure water. By calculating the steady-state concentration over a membrane under an oxygen gradient, we have shown that the oxygen storage capacity $S$ can be even more enhanced by stacking multiple bilayers, as is the case in myelin sheaths of axons in the nervous system. The stacking enhancement levels out when many membranes are stacked, meaning that beyond a certain number of stacked membranes, stacking even more would have limited efficiency. This could explain why myelin sheaths appear to consist of 10–300 stacked bilayers but not thousands. Finally, the enhancement is negatively affected by an increase of the aqueous phase between the bilayers, which can for instance occur in cancer cells with more disordered stacking geometry.

## References

1. Popel AS (1989) Theory of oxygen transport to tissue. Crit Rev Biomed Eng 17:257–321
2. Tsukihara T, Aoyama H, Yamashita E et al (1995) Structures of metal sites of oxidized bovine heart cytochrome c oxidase at 2.8 A. Science 269:1069–1074
3. Colliez F, Gallez B, Jordan BF (2017) Assessing tumor oxygenation for predicting outcome in radiation oncology: a review of studies correlating tumor hypoxic status and outcome in the preclinical and clinical settings. Front Oncol 7:10

4. Morell P, Quarles RH (1999) Characteristic composition of myelin. Basic Neurochem Mol Cell Med Asp 6:69–94

5. Arroyo EJ, Scherer SS (2000) On the molecular architecture of myelinated fibers. Histochem Cell Biol 113:1–18

6. Pias SC (2021) How does oxygen diffuse from capillaries to tissue mitochondria? Barriers and pathways. J Physiol 599:1769–1782

7. Dotson RJ, Smith CR, Bueche K et al (2017) Influence of cholesterol on the oxygen permeability of membranes: insight from atomistic simulations. Biophys J 112:2336–2347

8. Ghysels A, Krämer A, Venable RM et al (2019) Permeability of membranes in the liquid ordered and liquid disordered phases. Nat Commun 10:1–12

9. Ghysels A, Venable RM, Pastor RW, Hummer G (2017) Position-dependent diffusion tensors in anisotropic media from simulation: oxygen transport in and through membranes. J Chem Theory Comput 13:2962–2976

10. Hummer G (2005) Position-dependent diffusion coefficients and free energies from Bayesian analysis of equilibrium and replica molecular dynamics simulations. New J Phys 7

11. Krämer A, Ghysels A, Wang E et al (2020) Membrane permeability of small molecules from unbiased molecular dynamics simulations. J Chem Phys 153:124107

12. Brooks BR, Brooks CL III, Mackerell AD Jr et al (2009) CHARMM: the biomolecular simulation program. J Comput Chem 30:1545–1614

13. Klauda JB, Venable RM, Freites JA et al (2010) Update of the CHARMM all-atom additive force field for lipids: validation on six lipid types. J Phys Chem B 114:7830–7843

14. Vervust W, Ghysels A (2022) An electric RC circuit model to describe oxygen storage and transport in myelin sheaths. To be submitted

15. Mulkey DK, Henderson RA III, Olson JE et al (2001) Oxygen measurements in brain stem slices exposed to normobaric hyperoxia and hyperbaric oxygen. J Appl Physiol 90:1887–1899

16. Clever LH, Battino R, Miyamoto H et al (2014) IUPAC-NIST solubility data series. 103. Oxygen and ozone in water, aqueous solutions, and organic liquids (supplement to solubility data series volume 7). J Phys Chem Ref Data Monogr 43:33102

17. Molls M, Anscher MS, Nieder C, Vaupel P (2009) The impact of tumor biology on cancer treatment and multidisciplinary strategies. Springer

18. Vaupel P (2006) Abnormal microvasculature and defective microcirculatory function in solid tumors. In: Vascular targeted therapies in oncology. Wiley, pp 9–29

19. Payne SC, Bartlett CA, Harvey AR et al (2011) Chronic swelling and abnormal myelination during secondary degeneration after partial injury to a central nervous system tract. J Neurotrauma 28:1077–1088

20. Payne SC, Bartlett CA, Harvey AR et al (2012) Myelin sheath decompaction, axon swelling, and functional loss during chronic secondary degeneration in rat optic nerve. Invest Ophthalmol Vis Sci 53:6093–6101

21. Davoudi S, Ghysels A (2021) Sampling efficiency of the counting method for permeability calculations estimated with the inhomogeneous solubility–diffusion model. J Chem Phys 154:54106